05

Effective line X-ray generation by chirped femtosecond laser pulses interaction with copper target at local helium flow

© A.A. Garmatina[1], M.M. Nazarov[1], P.A. Shcheglov[1], M.V. Chaschin[1], V.A. Aleshkevich[2], B.G. Bravy[3], V.M. Gordienko[2], V.Yu. Panchenko[1]

[1] National Research Center „Kurchatov Institute“, Moscow, Russia
[2] Moscow State University, Moscow, Russia
[3] Department of Nanophotonics, Institute of Problems of Chemical Physics, Chernogolovka, Russia
e-mail: alga009@mail.ru

Received November 01, 2021
Revised December 12, 2021
Accepted December 30, 2021

Efficient laser-plasma line X-ray source was developed. X-ray generation was optimized by the laser pulse duration alteration and using the local helium blowing into the microplasma region on a copper target located in atmospheric conditions. Measured K_α x-ray flux of $2 \cdot 10^7$ ph/pulse/2π sr and conversion efficiency of 10^{-5} were achieved correspondingly.

Keywords: femtosecond laser pulses, X-rays.

DOI: 10.21883/EOS.2022.04.53728.64-21

Introduction

Currently, X-ray radiation is more and more widely used in solid-state physics, crystallography, microscopy, spectroscopy, visualization and for other analytical purposes [1–3]. It is essential that the papers focused on the investigations of condensed media in non-equilibrium states often only address relatively low-frequency atomic displacements. Ultrafast diffraction belongs to a family of techniques known as pump-probe techniques where two synchronized pulses are implemented. A femtosecond laser pulse responsible for initiating structural changes in the non-equilibrium state generation process may be used for pumping. In this case, trial emission is an ultrashort X-ray pulse which is dissipated from the exposed specimen in order to create a diffraction pattern. The achievements in the ultrafast structural behavior depend on how effectively the ultrashort pulses of hard spectrally intense X-ray radiation are generated. There is also a need for precision synchronization between probe and pump pulses. It should be noted that the atomic spatial resolution generally requires relatively hard X-ray radiation (with X-ray photon energy higher than 6 keV) that freely propagates in air. In order to solve the problems focused on the transient structural analysis and the generation of a diffraction pattern within a short (units of nanoseconds) period of time, a microplasma laser source with high characteristic X-ray photon output — about 10^8 ph/s - is required [1,3]. Laser plasma X-ray sources are generally obtained during focusing of high power pulse lasers on a target located in an evacuated chamber [3]. This approach has several disadvantages due to inevitable contamination of the chamber with flying target ablation products, bulky chambers and complicated automation. Therefore, a source placed outside the evacuated chamber is much more suitable. Moreover, gas atmosphere in front of the target will prevent dispersion of the ablation products and contamination of the focusing optics and other devices.

When the laser breakdown threshold is achieved, the air medium is ionized causing plasma generation, the medium refraction index is changed and conditions for defocusing, dissipation and loss of laser beam energy occur. All these factors cause restriction of the intensity delivered to the target and hence reduce the X-ray output. Plasma formation threshold may be increased by means of air replacement with gas with high ionization potential, for example, with helium [4]. This makes it possible to increase the delivered intensity and X-ray output during formation of a laser induced microplasma source. Thus, in [4], local helium injection into the beam waist area together with sharp focusing of a femtosecond laser beam with an aperture of NA~ 0.4 made it possible to achieve the copper K_α-photon (8 keV) output of about $2 \cdot 10^7$ ph/pulse/2π sr. But such scheme is not suitable enough for practical applications because at a short waist length, the X-ray signal is too sensitive to a non-ideal target location in the focal plane. Spatial restrictions on the placement of opto-mechanical elements in the scheme are also imposed. For example, of X-ray optic devices.

A scheme with weaker focusing and hence larger waist length will enable to form a laser plasma X-ray source which is less sensitive to the target position in the focal plane. We have demonstrated theoretically and confirmed experimentally in [5] that the use of chirped pulses in a NA ~ 0.1 scheme ensures increased X-ray output. It should be noted that we have already observed the X-ray output increase trend when using chirped femtosecond laser pulses earlier during the experiments with femtosecond filament acting on the metallic target placed in air [6].

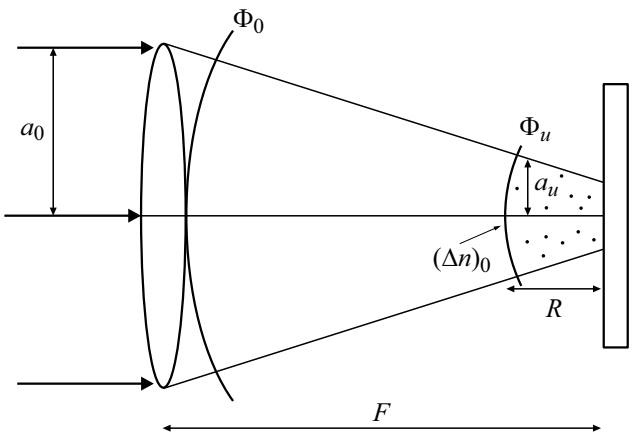

Figure 1. Diagram of interaction between a focused laser beam and target in ionization conditions.

The subject of the research is to develop a new approach to the effective generation of spectrally intense ultrashort X-ray radiation based on a solid-state laser plasma source. The use of titanium-sapphire laser system generating broadband pulses with the appropriate duration variation in the femto-picosecond range will enable to reduce the ionization loss, „bypass" the intensity restriction effect and achieve such energy density level when the characteristic X-ray photon flow achieves 10^8 ph/s. This meets the minimum requirements for most of applications.

Sharp focusing criterion

Effective X-ray generation method in normal ambient conditions involves minimized negative influence of laser-induced preplasma in the near-surface target region on the femtosecond laser intensity on the target itself. Intensity attenuation, firstly, is caused by the plasma ionization loss and, secondly, by the laser beam defocusing in plasma. In order to achieve the optimum laser impact conditions, focusing optics with high numerical aperture is required. In this case, the ionization process start may be decelerated and the ionized path length may be reduced accordingly due to the increased fluid ionization threshold, for example, when using helium [4]. A sharp focusing mode criterion when plasma beam defocusing can be suppressed is proposed herein using analytical estimations.

A collimated Gaussian light beam with an amplitude $A(r) = A_0 \exp(-r^2/a_0^2)$ incoming on a lens with a focal distance F obtains a curved phase front downstream of the lens $\Phi_0(r) = kr^2/(2F)$ (Fig. 1).

We assume that the effective plasma initiation takes place at some intensity on the beam axis I_{u0}. This will occur when the beam achieves a radius of a_u which is derived from the law of conservation of energy $I_0 a_0^2 = I_{u0} a_u^2$, where I_0 is the intensity on the axis of the beam incoming on the lens, R is the beam wave front curve radius, a_u id derived from $\frac{a_0}{F} = \frac{a_u}{R}$. Therefore, the beam phase front at the plasma medium inlet is described in this cross-section as follows

$$\Phi_u = \frac{kr^2}{2R}. \tag{1}$$

For ionization, plasma refraction index increment Δn by the end of pulse action in the same cross-section may written as follows

$$|\Delta n| = \text{const} \cdot I^{\gamma} = (\Delta n)_0 \exp\left(-\frac{2\gamma r^2}{a_u}\right),$$

where γ is the multiphoton ionization multiplicity. At the approach to the lens focus, phase incursion due to self-defocusing will be

$$\Phi_{nl} = k \int_0^R |\Delta n| dz.$$

For assessment, take Δn outside the integral sign because the plasma medium length is not large. Then

$$\Phi_{nl} = k|\Delta n|R \approx k(\Delta n)_0 R \exp\left(-\frac{2\gamma r^2}{a_u^2}\right). \tag{2}$$

It is evident that at $\Phi_u > \Phi_{nl}$ defocusing has no prominent influence on the beam propagation. To compare (1) and (2), write the last expression for the paraxial region:

$$\Phi_{nl} = k(\Delta n)_0 R \left(1 - \frac{2\gamma r^2}{a_u^2}\right).$$

A continuous phase incursion does not influence the beam defocusing therefore the weak nonlinear defocusing impact condition will be as follows

$$kr^2/(2R) > k(\Delta n)_0 R \left(2\gamma r^2/a_u^2\right).$$

Using $\text{NA} = (a_u/R) = (a/F)$, we will finally obtain

$$\text{NA} > 2(\gamma(\Delta n)_0)^{1/2}.$$

The last expression may be considered as a criterion to determine the best sharp focusing condition when nonlinear defocusing in plasma is low. Total single ionization (corresponding to the electron concentration $n = 2.5 \cdot 10^{19}\,\text{cm}^{-3}$) causes the refraction index to change by $\Delta n_0 = 7 \cdot 10^{-3}$ at a wavelength of 0,8,μm. In the assumption that helium with an ionization potential of 24.5 eV (for helium at this wavelength $\gamma = 16$) is the optimum medium surrounding the near-surface target layer, the optimum sharp focusing is implemented when NA$>$ 0.6.

Such numerical aperture is achieved experimentally by means of special short-focal lens through which transportation of energy higher than 2−3 mJ without laser emission spectrum distortion is difficult. Or laser beams with lager aperture shall be used. Such beams require corrective adaptive optics and high quality focuser. It shall be noted that the experimental study in [4] carried out using the

focusing optics with NA = 0.4 did not allow to achieve the anticipated optimum X-ray generation condition. In addition, the Rayleigh length at high NA values becomes so small that any potential target surface defects has no prominent influence on the X-ray signal consistency during microplasma generation. This may be essential for applications associated, for example, with X-ray diffraction tasks.

The experimental results of a non-vacuum approach to the effective laser-induced X-ray generation in a „soft" focusing mode are discussed below. This approach is based on the injection of helium having a high ionization potential and enabling to minimize the amount of induced electrons combined with the chirped pulse mode for optimization of energy delivery to the area of laser emission interaction with the substance.

Experimental setup

The experiments were performed using a Ti : Sa femtosecond laser system with two gain stages, the spectrally limited pulse length was 30 fs at 800 nm, the pulse energy was max. 6 mJ and the pulse repetition rate was 10 Hz. The pulse length was varied by varying the relative positions of lattices in the optical compressor and was controlled by SHG−FROG method. A laser beam with a FWHM of 1 cm was focused with the off-axis parabola (NA = 0.1) to achieve „soft" focusing on the moving surface of the copper target. The target was moved using vertically- and horizontally-aligned stepped motors. The target speed was chosen so that each next pulse can interact with a „new" target surface placed in air. To supply helium to the area of laser interaction with the target, a small tube was used which was made in a form of a silicon tube with its open ends oriented towards the target and hence towards the incident laser beam. The tube was filled with helium using a 0.4 mm syringe needle whose point was in the plasma initiation region in the target near-surface area. The tube walls provided gas accumulation in the are of laser emission interaction with the target. The needle was connected via a silicon tube to the helium bottle. Helium flow rate is these conditions did not exceed 0.25 l/min. The integrated X-ray radiation was recorded by 9107FLB photomultiplier tube with NaI scintillator and beryllium filter. The photomultiplier tube was placed 30 cm from the target. The X-ray spectra were measured using Amptek spectrometer. The spectrometer position was varied according to the X-ray flux so that to ensure single-photon measurement conditions. For helium injection, a 120 μm aluminum filter was also placed in front of the spectrometer. A second harmonic generation signal induced by the interaction between the focused laser emission and target was extracted using SZS 25 band pass filter and measured using Ocean Optics HR-400 spectrometer. For X-ray diffraction study, as setup was used which consisted of a lead diaphragm with dimensions 2×0.3 cm and a thickness of 12 mm. An X-ray photon beam passing the slit fell on the silicon crystal (111) turned at the Bragg angle to the incident radiation. The reflected radiation spectrum was recorded suing Amptek spectrometer. The experimental setup is shown in Fig. 2.

Experimental results

The experiments carried out in air and during helium injection investigated the characteristic X-ray output (8 keV) vs. the pulse length at fixed energy 6 mJ (vacuum intensity is $4 \cdot 10^{17}$ W/cm^2 at a spectrally limited pulse and $1.3 \cdot 10^{16}$ W/cm^2 at a pulse length of 1 ps) (Fig. 3, *a*). It was observed that the output was as low as possible in both cases at a spectrally limited pulse. The output grows nonlinearly with the pulse length increase. A small asymmetry is observed when using pulses with different sign of chirp — for positively chirped pulse, the X-ray output is about 1.5 times higher. In air with positively and negatively chirped pulse, the output grows significantly within 30−300 fs and then increases slowly and achieves its maximum value at a length of about 1 ps. In case of helium injection into the area of interaction between the laser beam and target, the signal amplitude is about 50 times higher compared with air.

The maximum X-ray output is also achieved in case of positively chirped pulse with a smaller length (300 fs). When using a negatively chirped pulse, the maximum X-ray output is about 1.5 times lower and corresponds to a larger pulse length (500 fs).

We have measured the characteristic X-ray spectra in air and helium (Fig. 3, *b*). The maximum output measured in air achieved $4 \cdot 10^5$ ph/pulse/2π sr. In helium injection conditions, this quantity grows and achieves $2 \cdot 10^7$ ph/pulse/2π sr. Conversion efficiency is 10^{-5}. The data is consistent with the known findings obtained in case of helium injection in sharp focusing mode [4]. This a record-setting conversion efficiency for a non-vacuum X-ray source.

In order to find the cause of such X-ray dependence on pulse length (and vacuum intensity variation), energy measurements were made on a laser beam focused in air and helium without a target to estimate the gas ionization loss. Diameters of craters obtained in the target were also measured for various laser pulse lengths in air and helium. It has been found that the loss in air at a spectrally limited pulse achieve 70% and drop down to about 30% at a pulse of about 1 ps. And the crater melt zone diameter achieves 100 μm in case of a positively chirped pulse with a length of 1 ps, which is significantly larger than the beam size measured without medium (vacuum conditions) in front of the target ($\sim 10\,\mu$m). Therefore, though the increase in pulse length during target exposure in air causes the decrease in medium ionization, complete suppression of ionization influence on beam defocusing is not possible. The intensity assessed on the target according to the crater

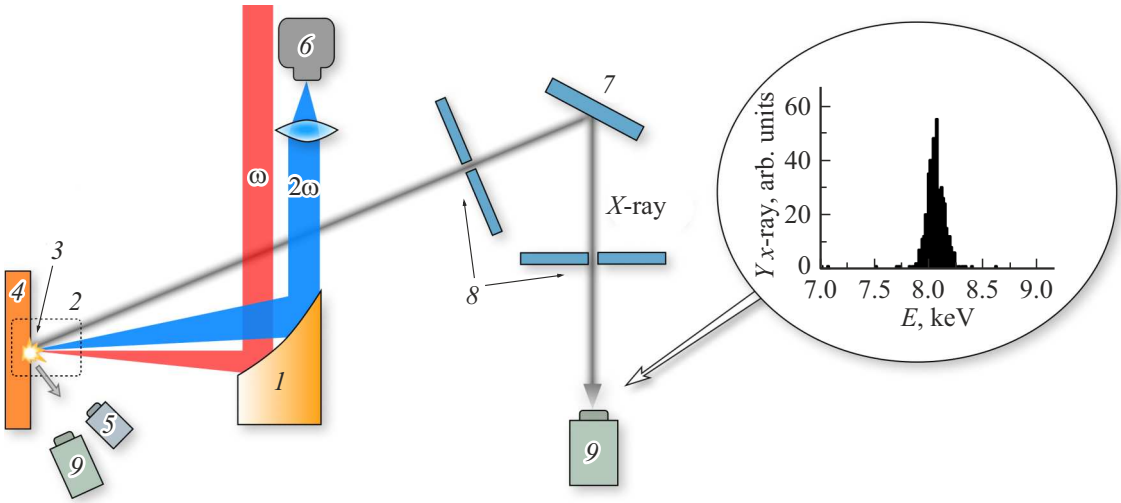

Figure 2. Experimental setup: *1* — off-axis parabola, *2* — silicon tube, *3* — needle for helium injection, *4* — copper target, *5* — photomultiplier tube, *6* — Ocean Optics fiber-optic spectrometer, *7* — silicon crystal (1,1,1), *8* — lead slit, *9* — Amptek spectrometer. The detail shows a characteristic spectrum shown after diffraction.

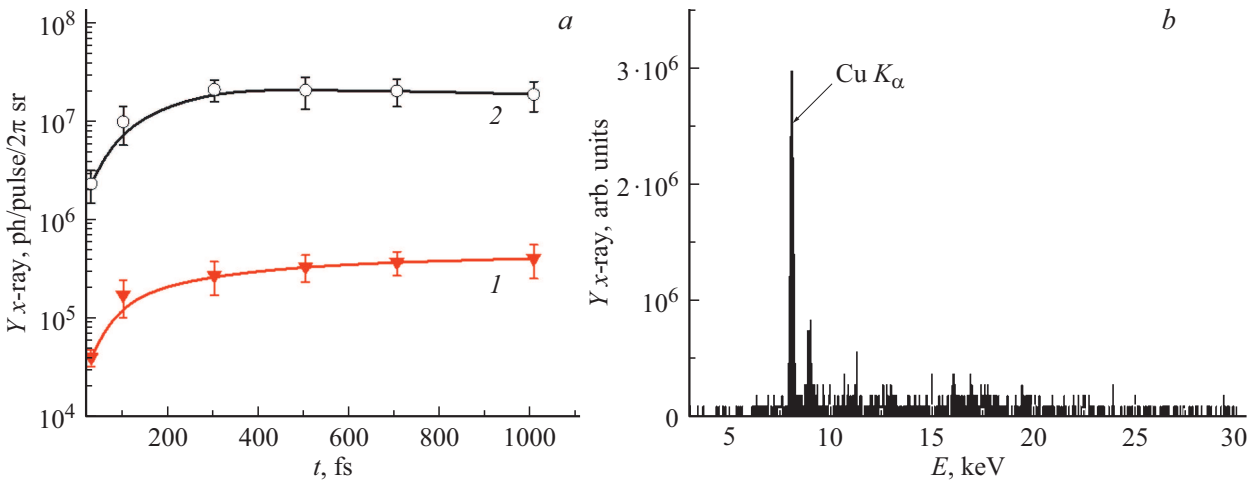

Figure 3. X-ray output vs. positive chirped pulse length in air (*1*) and helium (*2*) (*a*). X-ray spectrum of the target microplasma during helium injection (*b*).

diameter, laser energy and positively chirped pulse length (1 ps) is limited at max. $2 \cdot 10^{14}$ W/cm^2.

On the other hand, when a helium layer with a higher ionization potential is present in front of the target, ionization energy loss is about 30% at spectrally limited pulse and drop down to the level at which defocusing is not critical at a pulse length of about 300 fs. At the same time, the crater diameter is reduced from 100 μm at short pulse (30–100 fs) to 12 μm at a pulse length 300*to*700 fs (Fig. 4). Thus, the pulse length increase makes it possible to „bypass" the intensity limitation caused by the medium ionization and to achieve the quasi vacuum conditions when the medium ionization has a little if any effect on the interaction between the laser pulse and target.

Thus, with the pulse length increase, the crater diameter is reduced and the energy delivered to the target grows. Therefore, the energy density on the target is increased and apparently plays a key role in the X-ray output increase. However, the question regarding the intensity on the target which is responsible for the occurrence of hot electrons causing the X-ray generation remain open. It should be noted that similar measurements of X-ray output in vacuum conditions demonstrate the X-ray signal amplitude decay with the increase in the pulse length at the conservation of pulse energy [7].

It is known [8] that the intense femtosecond laser impact on a target in air can be also accompanied with second harmonic laser generation that depends on the intensity similar to the X-ray signal. Therefore, the experiments with helium injection involves simultaneous measurement of the second harmonic signal recorded in the target reflection direction. During interaction between the spectrally limited

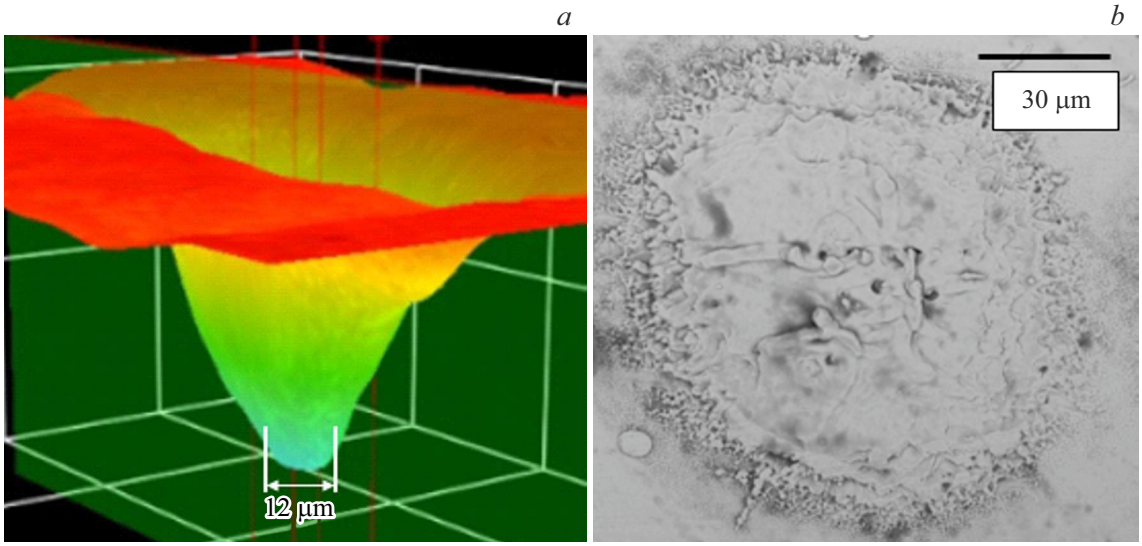

Figure 4. (*a*) Copper target crater image made at laser pulse lengths of 400 fs during helium injection using HRM-300 Series 3D microscope, nuclear size is 12 μm. (*b*) Crater image made at laser pulse lengths of 50 fs during helium injection using Phenom PRO-X scanning election microscope, melt diameter is 100 μm.

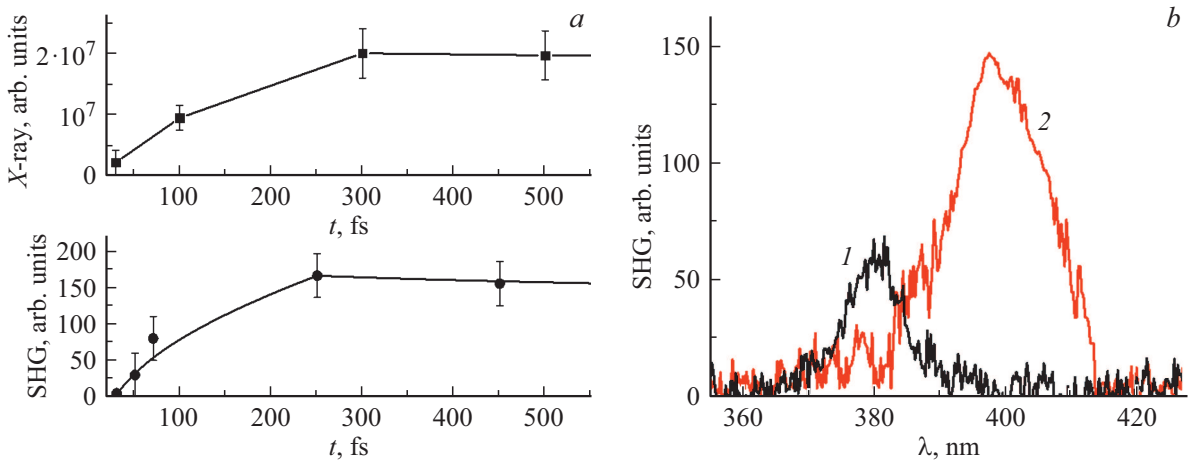

Figure 5. (*a*) X-ray and SHG signals vs. pulse length. (*b*) Second harmonic spectra at pulse lengths of 50 fs (*1*) and 400 fs (*2*).

pulse and target in helium environment, broadband plasma irradiation was observed and the second harmonic signal extraction was not possible. When the length was increased up to 50 fs, it was already possible to record the second harmonic spectrum. It spectrum was shifted by approx. 20 nm (Fig. 5, *b*) with respect to the spectrum recorded at 400–500 fs when plasma effect is low. Such shift may occur due to the refraction index variation caused by fast gas ionization by the pulse front and by the subsequent recombination process. This shift may be used to estimate electron concentration [9]:

$$N_e \approx \frac{2\pi m_e c^3 \Delta\lambda}{e^2 \lambda^3} \frac{\tau}{L},$$

where $\Delta\lambda$ is the second harmonic emission shift ($\Delta\lambda \sim 20$ nm), λ is the emission wavelength (in case of titanium-sapphire laser $\lambda = 0.8\,\mu$m), τ is the laser pulse length ($\tau = 50$ fs), L is the characteristic nonlinear interaction length (Rayleigh length of a laser beam focused by the parabola, $L \sim 30\,\mu$m). The electron concentration N_e is equal to $\sim 3 \cdot 10^{19}$ cm^{-3} and is responsible for full single ionization at the intensity of about 10^{15} W/cm^2 [4]. It has been found that the second harmonic signal behavior depending on the laser pulse length is similar to the X-ray behavior (Fig. 5, *a*). Since the second harmonic amplitude grows with the increase in pulse length, it is assumed that laser intensity also grows. However, the origin of such behavior requires additional analysis.

The crater diameter analysis results obtained at the pulse length of 50 fs (Fig. 4) which depends on the ionization loss (about 30%) and hence on the nonlinear defocusing also enable to estimate the intensity. It is about 10^{15} W/cm^2.

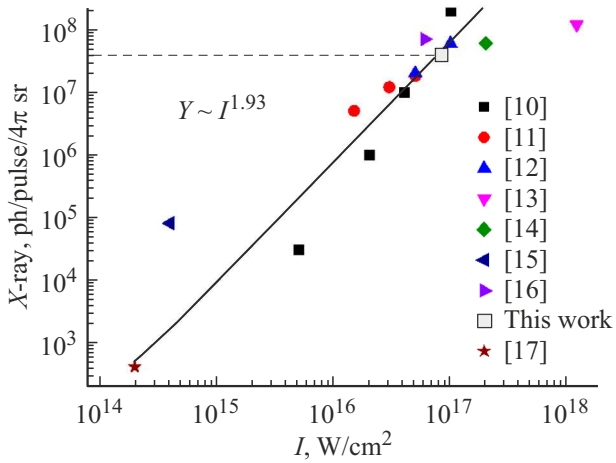

Figure 6. Characteristic X-ray photon output vs. vacuum laser intensity. The data has been obtained from the sources indicated in the Figure. The figure also shows the experiment result (grey box).

Fig. 6 shows a summary of the characteristic X-ray output depending on the laser intensity (from [10–17] for vacuum conditions and pulse length of 50−250 fs). The figure also shows the photon output (grey box) obtained in this experiment at the pulse length of 300 fs. The X-ray output dependence on the intensity is approximately quadratic. It should be noted that the intensity range $(0.4-0.8) \cdot 10^{17}$ W/cm^2 [10–14] corresponds to the X-ray output obtained in this experiment depending on the pulse length. This corresponds to the energy density variation within $(4-10) \cdot 10^3$ J/cm^2 [10–17].

The experiment carried out in helium at a pulse length of 300 fs, crater floor diameter of 12 μm and energy of about 5.5 mJ that has reached the crater floor (estimated including the measured ionization loss of max. 10%) can give the energy density of about $5 \cdot 10^3$ J/cm^2. This corresponds by order of magnitude with the energy density estimation in [12] that corresponds to the X-ray photon output at the pulse length of 45 fs. The estimated intensity is equal to $1.5 \cdot 10^{16}$ W/cm^2 which 5 times lower than in [12]. In our opinion this is indicative of the fact that the energy density (i.e. energy deposition) growing with the pulse length may play a significant role in the X-ray output increase. Additional investigations are required to obtain a more clear physical pattern.

It should be noted that according to the assumption in [16], the hot electron temperature decreases with the increase in the pulse length at fixed laser energy due to the reduced intensity. As a result the lateral dimension of the hot electron region is also reduced. The characteristic radiation source size is also reduced. Therefore, it is essential that it is the source size that determines the resolution for X-ray diffraction examination and phase-contrast visualization. On the other hand, if the energy applied to hot electrons remain the same with the pulse length growth, then the number of hot electrons is increased because the applied energy is now redistributed in the low-energy hot electron area [16]. Verification of these assumptions is the subject of further investigations.

The obtained 8 keV characteristic X-ray source was used in trial diffraction experiments with crystalline silicon (111). A high contrast copper line was extracted in a broadband X-ray spectrum. Diffracted X-ray photons on a specimen placed at the Bragg angle were recorded with high contrast (about 100) with respect to the background (detail in Fig. 2).

Thus, we have developed the experimental setup and investigated the laser plasma generation of ultrashort X-ray radiation. A procedure to determine laser intensity on a target has been developed and the appropriate measurements have been carried out. Approach to obtain characteristic X-ray radiation using chirped laser pulses generated in non-vacuum conditions has been described. The concept of characteristic X-ray radiation generated in non-vacuum has been described and makes it possible to obtain the output comparable with X-ray photon fluxes in synchrotrons, but with subpicosecond pulse length, when using femtosecond laser emission in high repetition rate conditions (1 kHz and higher).

Hopefully the developed non-vacuum approach to spectrally intense X-ray photon flux generation will be used in laboratories to solve the time-resolution X-ray diffraction diagnostics tasks.

Conclusion

A non-vacuum approach to effective laser generation of X-ray radiation is proposed. This approach is based on the injection of helium having a high ionization potential and enabling to minimize the amount of induced electrons combined with the chirped pulse mode for optimization of energy density in the area of laser emission interaction with the substance.

It has been observed that during the action of 6 mJ chirped femtosecond laser pulses focused (NA = 0.1) by the off-axis parabola on the copper target with helium injection into the interaction area, the X-ray output at a pulse length of 300-500 fs achieves its maximum value $2 \cdot 10^7$ ph/pulse/2π sr (or $2 \cdot 10^8$ ph/s/2π sr) which is the maximum value for non-vacuum conditions and meets the required diffraction experiment conditions.

When the target in helium injection conditions was exposed to focused femtosecond laser pulses, a second harmonic signal was recorded in the direction of mirroring from the target. When the laser pulse length was varied by means of chirping, the change in the second harmonic amplitude corresponds qualitatively to the X-ray output behavior. The blue shift of the harmonic spectrum at a pulse length of 50 fs was used to estimate the electron concentration in plasma which is equal to $3 \cdot 10^{19}$ cm^{-3} that

satisfies the total single ionization condition and hence the intensity of 10^{15} W/cm^2.

The obtained 8 keV characteristic X-ray source was used in trial diffraction experiments with crystalline silicon (111). A high contrast copper line was extracted in a broadband X-ray spectrum. Diffracted X-ray photons on a specimen placed at the Bragg angle were recorded with high contrast (about 100) with respect to the background.

Acknowledgments

The authors are grateful to N.V. Minaev for the assistance in image processing, to D.A. Sidorov-Biryukov and A.V. Mitrofanov for the assistance in the laser system setting.

Funding

This study was funded by the Ministry of Science and Higher Education of the Russian Federation under Agreement № 075-15-2021-1358 dated October 12 , 2021. (ID RF–0951.61321X0015).

Conflict of interest

The authors declare that they have no conflict of interest.

References

[1] G. Sciaini. Appl. Sci., **9** (7), 1427 (2019). DOI: 10.3390/app9071427
[2] G.V. Fetisov. Phys.-Usp., **63** (1), 2 (2020). DOI: 10.3367/UFNe.2018.10.038435
[3] M. Afshari, P. Krumey, D. Menn, M. Nicoul, et al. Struct. Dyn., **7** (1), 014301 (2020). DOI 10.1063/1.5126316
[4] B. Hou, J. Easter, A. Mordovanakis, K. Krushelnick, J.A. Nees. Opt. Expr., **16** (22), 17695–17705 (2008). DOI 10.1364/OE.16.017695
[5] A.A. Garmatina, B.G. Bravy, F.V. Potemkin, M.M. Nazarov, V.M. Gordienko. J. Phys.: Conf. Ser., **1692** (1), 012004 (2020). DOI: 10.1088/1742-6596/1692/1/012004
[6] A.A. Garmatina, M.M. Nazarov, I.A. Zhvaniya, V.M. Gordienko, V.Y. Panchenko. Las. Phys. Lett., **16** (2), 025401 (2019). DOI 10.1088/1612-202X/aaf6a2
[7] M.M. Nazarov, P.A. Shcheglov, M.V. Chaschin, A.A. Garmatina et al. J. Phys.: Conf. Ser., **1692** (1), 012018 (2020). DOI: 10.1088/1742-6596/1692/1/012018
[8] V.M. Gordienko, I.A. Zhvaniya, I.A. Makarov. Appl. Phys. A, **120** (2), 409–415 (2015). DOI: 10.1007/s00339-015-9202-4
[9] W.M. Wood, G. Focht, M.C. Downer. Opt. Lett., **13** (11), 984–986 (1988). DOI: 10.1364/OL.13.000984
[10] V. Arora, P.A. Naik, J.A. Chakera, S. Bagchi et al. AIP Adv., **4** (4), 047106 (2014). DOI: 10.1063/1.4870946
[11] M. Hada, J. Matsuo. Appl. Phys. B, **99** (1), 173–179 (2010). DOI: 10.1007/s00340-010-3902-4
[12] N. Zhavoronkov, Y. Gritsai, M. Bargheer, M. Woerner et al. Opt. Lett., **30** (13), 1737–1739 (2005). DOI:10.1364/OL.30.001737
[13] H. Wang, Z. Li, Z. Chen. Appl. Phys. B, **124** (9), 1-8 (2018). DOI: 10.1007/s00340-018-7039-1
[14] M. Iqbal, Z. Urrehman, H. Im, J.G. Son et al. Appl. Phys. B, **116** (2), 305–311 (2014). DOI: 10.1007/s00340-013-5691-z
[15] A. Baguckis, A. Plukis, J. Reklaitis, V. Remeikis et al. Appl. Phys. B, **123** (12), 1-7 (2017). DOI: 10.1007/s00340-017-6868-7
[16] R. Rathore, V. Arora, H. Singhal, T. Mandal et al. Laser and Particle Beams, **35** (3), 442-449 (2017). DOI:10.1017/S026303461700043X
[17] M. Hagedorn, J. Kutzner, G. Tsilimis, H. Zacharias. Appl. Phys. B, **77** (1), 49-57 (2003). DOI: 10.1007/s00340-003-1226-3